Detecting precancerous lesions in the hamster cheek pouch using spectroscopic white-light optical coherence tomography to assess nuclear morphology via spectral oscillations

Robert N. Graf
Duke University
Department of Biomedical Engineering
136 Hudson Hall
Durham, North Carolina 27708

Francisco E. Robles
Duke University
Department of Biomedical Engineering
and
Department of Medical Physics
2424 Erwin Road, Suite 101
Durham, North Carolina 27708

Xiaoxin Chen
North Carolina Central University
Julius L. Chambers Biomedical/Biotechnology Research Institute
1801 Fayetteville Street
Cancer Research Program
Durham, North Carolina 27707

Adam Wax
Duke University
Department of Biomedical Engineering
136 Hudson Hall
and
Department of Medical Physics
2424 Erwin Road, Suite 101
Durham, North Carolina 27708

Abstract. We have developed a novel dual-window approach for spectroscopic optical coherence tomography (OCT) measurements and applied it to probe nuclear morphology in tissue samples drawn from the hamster cheek pouch carcinogenesis model. The dual-window approach enables high spectral and depth resolution simultaneously, allowing detection of spectral oscillations, which we isolate to determine the structure of cell nuclei in the basal layer of the epithelium. The measurements were executed with our parallel frequency domain OCT system, which uses light from a thermal source, providing high bandwidth and access to the visible portion of the spectrum. The structural measurements show a highly statistically significant difference between untreated (normal) and treated (hyperplastic/dysplastic) tissues, indicating the potential utility of this approach as a diagnostic method. [DOI: 10.1117/1.3269680]

Keywords: spectroscopy; optical coherence tomography; light scattering spectroscopy; early cancer detection; nuclear morphology.

Paper 09263R received Jun. 24, 2009; revised manuscript received Oct. 8, 2009; accepted for publication Oct. 9, 2009; published online Dec. 16, 2009.

1 Introduction

Cancers typically develop slowly over time, beginning with just a few abnormal cells that grow and proliferate. The majority of malignancies develop through precancerous states characterized by varying levels of architectural and cytologic abnormality.[1] Detecting these structural changes in tissues at the earliest possible stages could provide an increased opportunity for therapeutic intervention and thus, greatly reduce rates of mortality and morbidity. However, detecting precancerous development is a great challenge for available screening techniques.

The current gold standard for detecting cancer of epithelial tissues is the histopathologic analysis of biopsy samples. Biopsy samples are excised from the tissue under examination and then fixed, sectioned, stained, and ultimately examined by a pathologist for morphological abnormalities. Although this procedure is the standard practice for cancer diagnosis, there are several drawbacks to this approach, including the subjectivity of diagnoses, the inherent invasiveness of biopsies, the time delay between biopsy and diagnosis, and the poor coverage of at-risk tissue.

It is clear that improved screening and diagnostic technologies are needed to overcome these limitations. In recent years, large amounts of research have focused on developing optical methods for early cancer detection[2–4] because such methods hold great promise to overcome the limitations of the traditional biopsy listed earlier. One specific technique, elastic light scattering spectroscopy, is an optical technique that analyzes scattered light to obtain information about the structures with which the light interacts. For decades, elastic light scattering has been utilized in a variety of applications where direct measurement of physical properties is impractical or impossible. Most recently, advances in biophotonics have enabled application of elastic light scattering to biology and medicine. Using powerful, broadband light sources, elastic scattering spectroscopy (ESS) has been used by several

Address all correspondence to: Adam Wax, Duke University, Department of Biomedical Engineering, 136 Hudson Hall, Durham, North Carolina 27708. Tel: 919-660-5143; Fax: 919-684-4488; E-mail: a.wax@duke.edu

1083-3668/2009/14(6)/064030/8/$25.00 © 2009 SPIE

groups to investigate the cellular morphology of *in vivo* and *ex vivo* tissue samples.[5–8] Because enlargement of the nuclear diameter is a key indicator of precancerous growth,[1] the morphology of the cell nucleus has become a strategic target for light scattering studies.

These advancements have paved the way for a new elastic light scattering technique known as Fourier domain low-coherence interferometry (fLCI).[9,10] The fLCI approach uses interferometry to obtain depth-resolved spectroscopic information that can then be analyzed to recover structural information, such as nuclear morphology, from specific layers in a sample. For early cancer detection, fLCI may be applied to detect enlargement of nuclear diameter, which can serve as a biomarker of precancerous transformation. This biomarker, either alone or in conjunction with other information derived from the light scattering signal, can provide the quantitative information necessary to distinguish between normal and dysplastic epithelial tissue with high sensitivity and specificity.

In this paper, we present the results of the first study assessing the ability of the fLCI technique to distinguish between normal and dysplastic *ex vivo* epithelial tissues. In the study, quantitative nuclear morphology measurements are used as a biomarker to distinguish between normal and dysplastic hamster cheek pouch epithelium.

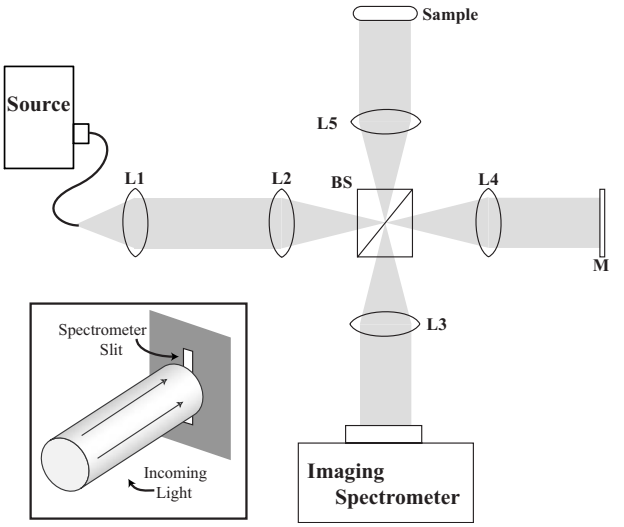

Fig. 1 Schematic of the pfdOCT system. Light source—250-W Xe arc-lamp. L1 through L5—lenses. BS—beamsplitter. M—reference mirror. Inset: Incoming light incident on the spectrometer slit. Slit allows only a small slice of incoming light to enter the imaging spectrometer. Adapted from Ref. 11.

2 Materials and Methods

2.1 *Animal Model*

The animal study was completed using the hamster cheek pouch carcinogenesis model. For the animal study, all experimental protocols were approved by the Institutional Animal Care and Use Committees of Duke University and North Carolina Central University and in accordance with the National Institutes of Health (NIH). Male Syrian golden hamsters, six weeks of age, were obtained from Harlan Laboratories (Indianapolis, Indiana) and housed at North Carolina Central University. The animals were housed four per cage in a room with controlled temperature and humidity and in a 12-h light/dark cycle. Regular cage changes ensured maintenance of hygienic conditions. All animals were given the AIN-93M diet (Research Diets, New Brunswick, New Jersey). The diet consisted of 14% casein, 0.18% l-cystine, 49.5% corn starch, 12.5% maltodextrim 10, 10% sucrose, 5% cellulose, 4% soybean oil, 0.0008% t-Butylhydroquinone, 3.5% mineral mix, 1% vitamin mix, and 0.25% choline bitartrate. Tap water was available *ad libitum*. After an acclimatization period of one week, the left cheek pouch of each animal was topically treated with 100 μl of 0.5% 7,12-dimethylbenz[a]anthracene (DMBA; Sigma Chemical Company, St. Louis, Missouri) in mineral oil with a paintbrush three times per week for six weeks. The right cheek pouch was left untreated and served as the control group.

2.2 *Experimental Protocol*

At 24 weeks after the initial treatment of DMBA, the hamsters were shipped to Duke University for optical spectroscopic analysis. The hamsters were euthanasia by CO_2 asphyxiation before being subjected to gross necropsy. The entire left and right cheek pouches were excised and cut into two pieces. The samples were laid flat between two coverglasses, moistened with phosphate buffered saline (PBS), and immediately scanned by the parallel frequency domain optical coherence tomography (pfdOCT) system. Following the optical measurements, scanned areas were marked with India ink and the tissue samples were fixed in 10% PBS buffered formalin. The fixed samples were later embedded in paraffin, sectioned, and stained with hematoxylin and eosin (H&E) for histopathological analysis.

The complete animal trial analyzed tissue samples from 21 hamsters. Although one treated and one untreated sample were extracted from each animal and scanned by the fLCI system, only 16 of 21 untreated samples were used in the study. The signal-to-noise ratio of the scans from the remaining five untreated samples was insufficient to provide useful data. Therefore, these scans were not included in the spectroscopic analysis.

2.3 *Parallel Frequency Domain Optical Coherence Tomography*

Ex vivo tissue samples were examined using the pfdOCT system first described by Graf et al.[11] The pfdOCT system, shown in Fig. 1, is based on a modified Michelson interferometer geometry and utilizes a 4f interferometer first demonstrated by Wax et al.[12] The system utilizes a Xenon arc-lamp source (150 W, Newport Oriel, Stratford, Connecticut) for illumination, and the 4f interferometer uses two 4f imaging systems to spatially resolve light from the source to the detector. The detection plane of the imaging system coincides with the entrance slit of an imaging spectrometer (Shamrock 303i, Andor Technology, South Windsor, Connecticut), which spatially resolves 255 detection channels, each 25 μm in width. The imaging spectrometer optics, along with the combination of the 600 lines/mm grating and the 1024-pixel CCD array, limits the detected spectrum to the 500- to 625-nm range. Data from the spectrometer is downloaded in real time to a laptop PC via the USB 2.0 interface, and spectrometer control and data acquisition is achieved us-

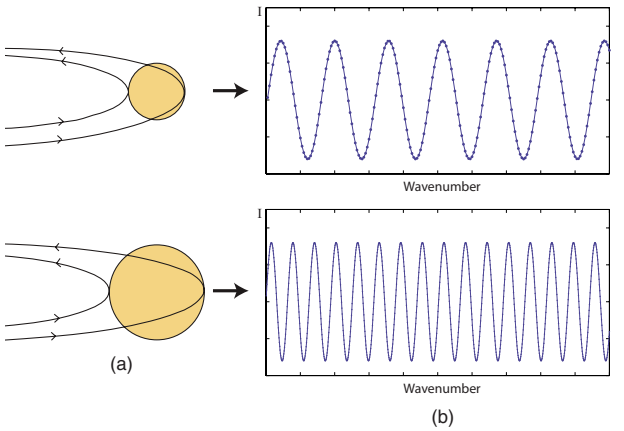

Fig. 2 (a) Cell nuclei with incident and scattered fields indicated. (b) Interference spectra with wave number–dependent oscillations caused by interference between front and back surface reflections.

ing custom LabVIEW (National Instruments, Austin, Texas) software.

The fLCI method seeks to recover structural information about scatterers by examining the wavelength dependence of the intensity of elastically scattered light. The technique determines scatterer sizes by analyzing the Fourier transform of the spectra originating from specific subsurface layers of a sample. Depth resolution is obtained by employing the coherence gating methods commonly used in frequency domain OCT. By exploiting the low temporal coherence length of a broadband light source in an interferometry scheme, fLCI can selectively analyze spectral information from the most diagnostically relevant layers in probed samples.

In order to perform depth-resolved spectroscopy, fLCI data must be processed to simultaneously obtain depth resolution *and* spectral resolution, from data acquired in a single domain. To implement this processing, fLCI and spectroscopic OCT (SOCT) have typically employed a short-time Fourier transform (STFT) in which a Gaussian window is applied to the interference signal before taking a Fourier transform, yielding a depth scan centered about a particular center wave number. By shifting the center of the Gaussian window and repeating the process, a data set with both depth and spectral resolution can be generated. It should be noted, however, that with this approach, any attempt to increase spectral resolution results in degradation of depth resolution and vice versa. Most recently, Robles et al. introduced the dual window (DW) method for processing SOCT signals, which can be incorporated into the fLCI analysis.[13] The DW method is based on performing two separate STFTs and combining the results to achieve simultaneously high depth and spectral resolution.

From the depth-resolved spectroscopic information, fLCI seeks to determine structural information by analyzing oscillations in the spectrum of light returned from a specific depth of interest. More specifically, fLCI seeks to distinguish between normal and dysplastic epithelial tissue by detecting the nuclear enlargement that occurs at the earliest stages of precancerous development. Figure 2(a) shows an illustration representing two nuclei as well as the scattering events that take place at both the front and back surfaces of each nucleus where an index of refraction change is present. Depending on the coherence of the field induced by the sample,[14] the reflections from the front and back surfaces of the nuclei will interfere with one another, producing constructive or destructive interference, as shown in Fig. 2(b). The frequency of this oscillation is directly dependent on the diameter and refractive index of the scatterer, with larger particles resulting in a higher frequency of oscillation and smaller particles resulting in a lower frequency of oscillation. The fLCI method seeks to detect and analyze these spectral oscillations to measure nuclear diameter.

2.4 *Data Processing*

The raw data acquired by the pfdOCT system consisted of 120 spectra, each of which originates from adjacent 25-μm-diam spatial points on the experimental sample. The raw data, along with the plots of three such spectra, are shown in Fig. 3(a). The diameter of the signal beam was shaped to illuminate only 120 of the 255 spectral channels of the imaging spectrometer to preserve the signal-to-noise ratio of the measurements.

To analyze spectra from specific tissue layers, the spectrum detected by each channel of the imaging spectrometer was processed using the DW processing method.[13] Briefly, the DW method uses the product of two STFTs to reconstruct the time-frequency distribution (TFD) of the interferometric signal: one STFT with a narrow window for high spectral resolution and another with a wide window for high spatial resolution. Equation (1) gives a mathematical description of the distribution obtained with the DW method from a single spatial line:

$$DW(k,z) = \int 2\langle E_S\rangle \cos(\kappa_1 \cdot \Delta OPL)\exp\left[-\frac{(\kappa_1 - k)^2}{2a^2}\right] \times \exp(-i\kappa_1 z)\mathrm{d}\kappa_1 \times \int \left\{2\langle E_s\rangle \cos(\kappa_2 \cdot \Delta OPL) \times \exp\left[-\frac{(\kappa_2 - k)^2}{2b^2}\right]\exp(-i\kappa_2 z)\right\}\mathrm{d}\kappa_2, \quad (1)$$

with a and b given as the standard deviations of the windows. In this particular arrangement, the spectral resolution is limited by the actual resolution of the spectrometer used, while the depth resolution is limited by the coherence length of the detected light.

Robles et al. have shown that the distribution obtained from the DW method can be related to Cohen's class of bilinear functions,[13] even though it is constructed using two linear operations. In one limit, where $a^2/b^2 \ll 1$, the DW distribution gives a measurement of the Wigner time-frequency distribution (TFD) with spectral and depth resolution set independently by the width of the two orthogonal windows, a and b. Significantly, the use of the two orthogonal windows eliminates many common artifacts in other TFDs, such as the cross-term artifacts from the Wigner TFD and the reflections in time artifacts from the Margenau and Hill TFD.[13] Further, the DW contains local oscillations in the spectral dimension that reveal morphological information about the sample—specifically, the distance between scattering surfaces in the vicinity of the point of analysis.

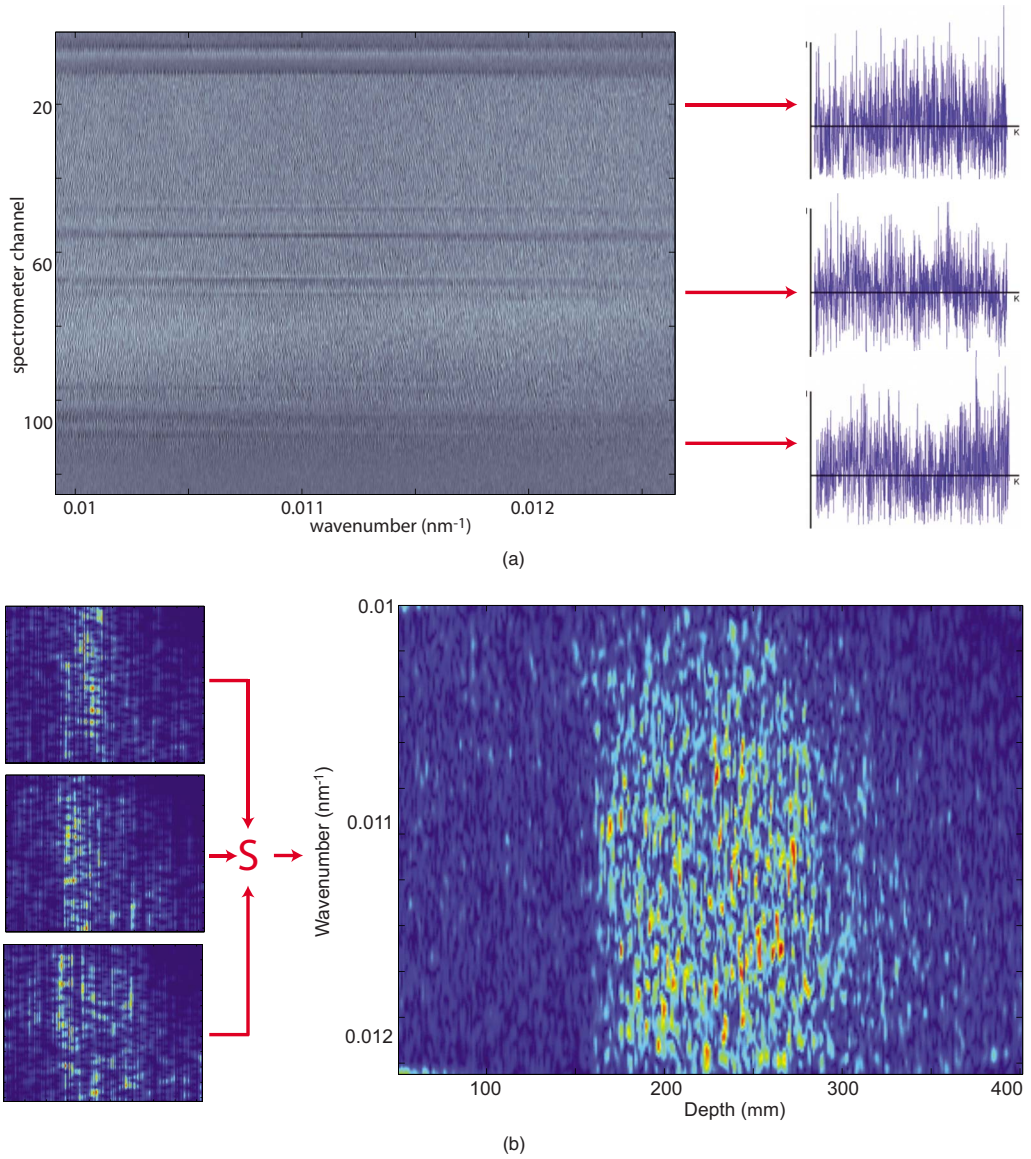

Fig. 3 (a) Raw data from the complete animal trial with spectra from three spectrometer channels shown. (b) Three typical depth-resolved spectroscopic plots produced by DW processing the spectra in (a). Summing the plots from all 120 channels produces the final TFD, as shown.

The DW method was implemented using a custom MATLAB program to process the data with both a narrow spectral window of 0.0405 μm^{-1} FWHM and a wide spectral window of 0.665 μm^{-1} FWHM. The depth-resolved spectra generated by each window were multiplied together to produce a plot with simultaneously high spectral and depth resolution. The resulting 120 depth-resolved spectroscopic plots were summed together to improve the signal-to-noise ratio, producing a single depth-resolved spectroscopic plot for each tissue sample, as shown in Fig. 3(b).

In neoplastic transformation, nuclear morphology changes are first observed in the basal layer of the epithelial tissue. In hamster buccal pouch tissue, the basal layer lies approximately 30 to 50 μm beneath the surface for normal tissue, and approximately 50 to 150 μm beneath the surface for dysplastic tissue. Because examination of the basal layer offers the earliest opportunity for detecting developing dysplasia, it is the target tissue layer for the fLCI technique and for this study.

In order to target the basal layer of the epithelium, the raw experimental data were first processed to yield a pfdOCT image by a line-by-line Fourier transform. These B-mode images were summed across the transverse axis to generate single depth plots (A-scan) like those presented in Fig. 4. Several important histological features can be identified in the depth scans and co-registered with the corresponding histopathology images. Figure 4 indicates the location of a keratinized layer (green arrow), the basal layer of the epithelium (red arrow), and the underlying *lamina propria* (blue arrow) in the micrographs of fixed and stained histological sections from untreated and treated tissue samples. Scattering peaks corresponding to the same tissue layers were identified in each depth scan. To correlate the distances in the histology images with distances in the depth scans, the index of refraction of

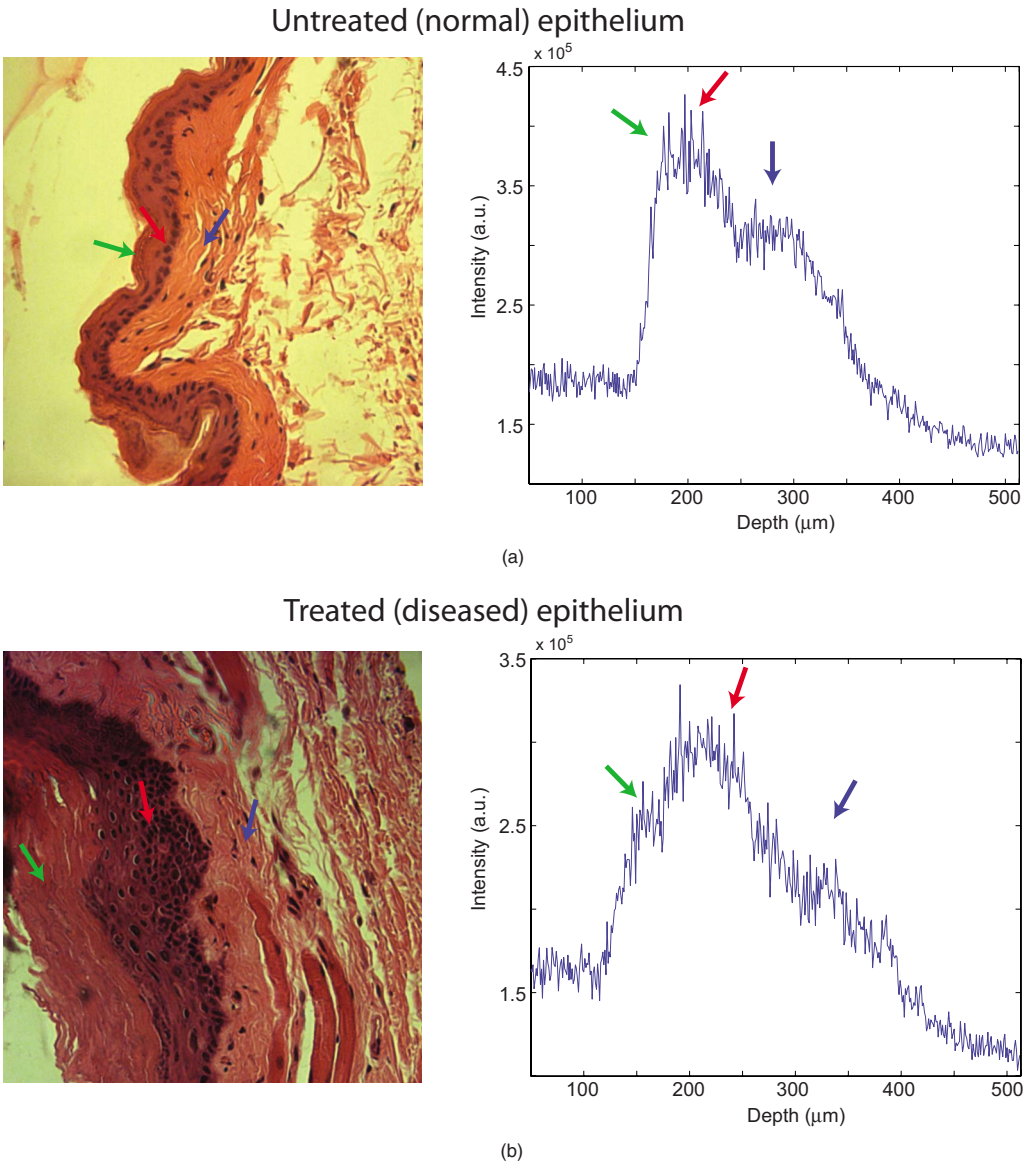

Fig. 4 Histopathology image and corresponding depth plot for (a) untreated and (b) treated epithelium. Arrows indicate keratinized layer (green), basal layer (red), and *lamina propria* (blue). (Color online only.)

the tissue was taken into account. An average refractive index for the tissue of $n=1.38$ was used to convert depth scan distances to optical path lengths.[15,16] Variation of the refractive index within the tissue is a potential limitation of the current method and is discussed further in the following.

For each sample, a 15-μm-depth segment corresponding to the location of the basal layer was selected from the depth scan and used to guide analysis of the depth-resolved spectroscopic plot, as shown in Fig. 5(a). The spectra from the depth identified with the basal layer in each A-scan were averaged to generate a single spectrum for light scattered by the basal layer. As shown in Fig. 5(b), a power law curve of the form $y=b\cdot x^{\alpha}$ was initially fit to each spectrum, modeling the spectral dependence resulting from the fractal structure of cellular organelles,[17–19] including heterogeneity of the substructure of the nucleus. The residual of each spectrum was calculated by subtracting the power-law curve from the experimental spectrum to produce a normalized spectrum that isolates the oscillatory features, as shown in Fig. 5(c).

The normalized spectra showed clear oscillations resulting from interference produced by scattering from the front and back surfaces of basal cell nuclei. Each normalized spectrum was Fourier transformed to generate a correlation plot similar to that shown in Fig. 5(d), which shows a clear peak corresponding to the dominant frequency in the normalized spectrum. Peak detection was carried out by an automated, custom MATLAB program (Mathworks, Natick, Massachusetts). The script first high-pass filtered the spectrum with a cutoff of four cycles in order to remove any low-frequency content not removed by the power-law fit. The location of the peak in the correlation plot was then automatically detected by the MATLAB script and related to scatterer diameter with the simple equation $d=\text{correlation distance}/(2\cdot n)$, where n is the refractive index, and d is the diameter of the cell nuclei. An

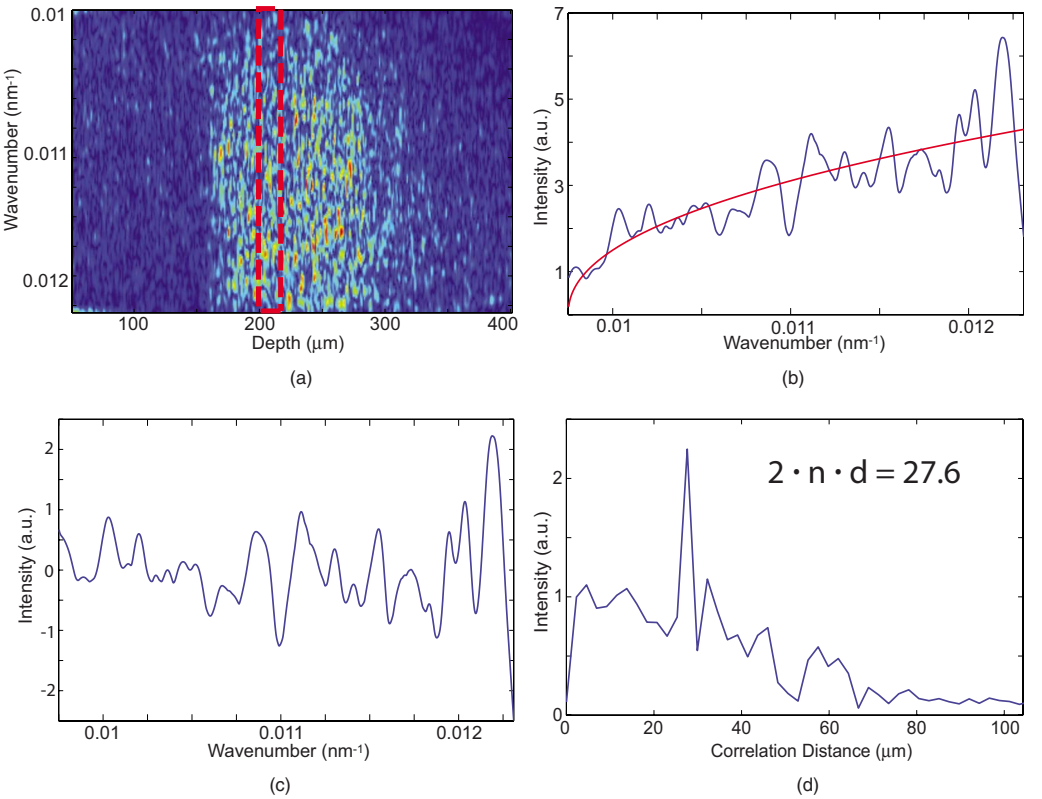

Fig. 5 (a) Depth-resolved spectroscopic plot with basal layer indicated by dashed red box. (b) Spectrum from basal tissue layer along with power-law fit. (c) Residual spectrum from basal tissue layer. (d) Correlation plot generated by Fourier transforming spectrum in (c). Peak correlation distance can be related directly to scatterer size. (Color online only.)

nuclear index of refraction of $n=1.395$ was assumed.[9]

3 Results

The results of the complete animal trial are summarized in Table 1 and presented graphically in Fig. 6. The 16 untreated tissue samples had a mean basal layer nuclear diameter of 4.28 μm with a standard deviation of 0.69 μm. The 21 treated tissue samples had a mean basal layer nuclear diameter of 9.50 μm with a standard deviation of 2.08 μm. A statistical t-test revealed a p-value of less than 0.0001, indicating a highly statistically significant difference between the basal layer nuclear diameters of the two populations. Histological analysis revealed that untreated samples appeared as unaltered epithelium, while the treated samples all showed a diseased tissue state ranging from inflammation and hyperplasia to dysplasia.

Figure 6 plots each treated (blue square) and untreated (red x) tissue sample as a function of its measured basal layer

Table 1 Summary of nuclear diameter measurements from the complete animal trial.

	Untreated	Treated
n	16	21
Mean (μm)	4.28	9.50
Std. dev	0.69	2.08
	p-value <0.0001**	

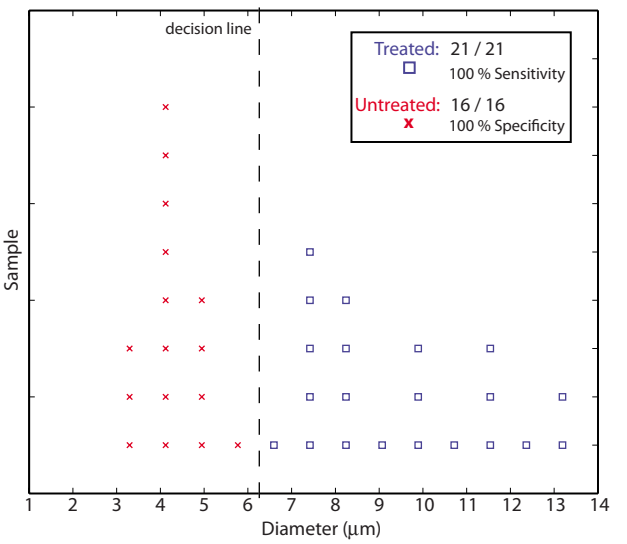

Fig. 6 Nuclear diameter measurements for each sample of the complete animal trial. The decision line results in 100% sensitivity and 100% specificity.

nuclear diameter. The presented decision line results in excellent separation between the normal and diseased samples. Using the indicated decision line, the study results correctly categorize 21 of 21 treated samples, providing 100% sensitivity, and correctly categorize 16 of 16 untreated samples, providing 100% specificity.

4 Discussion

The experimental results of the complete animal trial show that fLCI has great potential as a technique for distinguishing between normal and dysplastic epithelial tissues. Experimental measurements showed an excellent ability to precisely and accurately distinguish between treated and untreated animal tissue using *in situ* measurements of nuclear diameter as a biomarker. The measured diameters correspond nicely with the nuclear diameter expected for the basal tissue layer of hamster cheek pouch epithelium[20] when measurements are adjusted to account for fLCI's measurement of the minor axis of cell nuclei.[9] It should be noted that the development of dysplasia results in thickening in the basal tissue layer and a breakdown of cellular organization. As a result, fLCI measurements likely probe the major axis of some nuclei in diseased tissue, further contributing to the detected nuclear enlargement when compared with normal tissue.

The use of the DW method to extract depth-resolved spectra from animal tissue data is an important advance. The DW processing method permitted the measurement of spectral oscillations induced by nuclear scattering that could not be detected in data processed with the STFT. The fLCI data processed with the STFT suffers from an inherent tradeoff between spectral resolution and depth resolution. As a result of this trade-off, achieving an acceptable spectral resolution necessarily requires the degradation of depth resolution to the point that spectral oscillations induced by nuclear scattering are washed out. This washout is likely due to phase and frequency differences in the spectra originating from the different tissue layers that were combined as a result of the poor depth resolution. In contrast, the DW method produced depth-resolved spectroscopic plots with simultaneously high depth and spectral resolutions. The DW method generated satisfactory spectral resolution while maintaining high depth resolution, therefore permitting the spectral analysis of thin tissue segments. By avoiding the unwanted combination of signals from many tissue layers, the oscillatory components of spectra originating from the basal tissue layer were preserved and available for analysis.

Although the results of the animal study are extremely promising, the current methods are not without limitation. The dependence on refractive index in selecting tissue layers of interest is a challenge that must be further examined in the future. The current fLCI data processing algorithm does not account for potential variations of refractive index within a tissue. The current method also does not adjust for potential index changes induced by the onset of dysplasia, which also may be a confounding factor. In order to accurately measure optical path lengths within a tissue sample, a dynamic model of refractive index must be developed. Similarly, a robust method to account for the varying thickness and location of the basal layer during neoplastic transformation should be implemented.

Additionally, a more complex model of scatterers within the tissue should be developed for future studies. Other light scattering research[21–23] indicates that, in addition to spectral modulations, spectral shape can yield insight into tissue microarchitecture and health. Developing a light scattering model that can capture this information will be a priority as the fLCI technology is further developed.

Although the detection of peaks in the correlation plots for this study was automated to eliminate bias, subsequent analysis of the correlation data revealed that some plots contained multiple prominent peaks. Understanding how correlations between neighboring cellular structures and correlations between tissue layers contribute to generated correlation plots will facilitate the development of an advanced scattering model.

We are confident that the correlation peak represents nuclear diameter, as opposed to the separation between nuclei, for three primary reasons. First, the front and back surfaces of each nucleus are relatively well aligned for interference in the axial direction, whereas the alignment between different nuclei is not as well ordered and therefore less likely to produce oscillations in the spatially averaged spectrum. Second, because the distances between nuclei would have a much larger variation than the diameters of individual nuclei, we would expect the separation between nuclei to yield a much broader distribution of distances rather than the narrow correlation peaks seen in the correlation plots. Last, this study finds that the correlation peak shifts to longer distances for treated (diseased) samples while remaining at smaller distances for normal samples. This finding is consistent with the measurement of nuclear enlargement seen in hyperplastic and dysplastic tissues. On the other hand, if the correlation plot was measuring nucleus-to-nucleus correlation, we would expect to see the peak shift to *smaller* distances in diseased tissue due to the increase in nucleus-to-cytoplasmic ratio observed in dysplastic tissue.

5 Conclusion

The results of this study demonstrate fLCI's ability to distinguish between normal and diseased (DMBA-treated) epithelial tissue with high sensitivity and high specificity. The *in situ* nuclear morphology measurements are acquired without the need for exogenous staining agents or fixatives. The ability of the fLCI technique to make quantitative nuclear morphology measurements demonstrates its potential as an effective technology for noninvasively detecting dysplasia using an optical measurement. The results of these experiments lay the groundwork for further development of fLCI into a technique for clinical diagnostic applications such as the detection of early cancer development.

Acknowledgments

This research has been supported by grants from the National Institutes of Health (NCI R21-CA120128) and the National Science Foundation (BES 03-48204).

References

1. V. Kumar, A. K. Abbas, N. Fausto, S. L. Robbins, and R. S. Cotran, *Robbins and Cotran Pathologic Basis of Disease*, Elsevier/Saunders, Philadelphia (2005).

2. M. Panjehpour, B. F. Overholt, T. VoDinh, R. C. Haggitt, D. H. Edwards, and F. P. Buckley, "Endoscopic fluorescence detection of high-grade dysplasia in Barrett's esophagus," *Gastroenterology* **111**(1), 93–101 (1996).
3. C. Kendall, N. Stone, N. Shepherd, K. Geboes, B. Warren, R. Bennett, and H. Barr, "Raman spectroscopy, a potential tool for the objective identification and classification of neoplasia in Barrett's oesophagus," *J. Pathol.* **200**(5), 602–609 (2003).
4. P. R. Pfau, M. V. Sivak, A. Chak, M. Kinnard, R. C. K. Wong, G. A. Isenberg, J. A. Izatt, A. Rollins, and V. Westphal, "Criteria for the diagnosis of dysplasia by endoscopic optical coherence tomography," *Gastrointest. Endosc.* **58**(2), 196–202 (2003).
5. L. T. Perelman, V. Backman, M. Wallace, G. Zonios, R. Manoharan, A. Nusrat, S. Shields, M. Seiler, C. Lima, T. Hamano, I. Itzkan, J. Van Dam, J. M. Crawford, and M. S. Feld, "Observation of periodic fine structure in reflectance from biological tissue: a new technique for measuring nuclear size distribution," *Phys. Rev. Lett.* **80**(3), 627–630 (1998).
6. V. Backman, M. B. Wallace, L. T. Perelman, J. T. Arendt, R. Gurjar, M. G. Muller, Q. Zhang, G. Zonios, E. Kline, T. McGillican, S. Shapshay, T. Valdez, K. Badizadegan, J. M. Crawford, M. Fitzmaurice, S. Kabani, H. S. Levin, M. Seiler, R. R. Dasari, I. Itzkan, J. Van Dam, and M. S. Feld, "Detection of preinvasive cancer cells," *Nature (London)* **406**(6791), 35–36 (2000).
7. M. B. Wallace, L. T. Perelman, V. Backman, J. M. Crawford, M. Fitzmaurice, M. Seiler, K. Badizadegan, S. J. Shields, I. Itzkan, R. R. Dasari, J. Van Dam, and M. S. Feld, "Endoscopic detection of dysplasia in patients with Barrett's esophagus using light-scattering spectroscopy," *Gastroenterology* **119**(3), 677–682 (2000).
8. I. Georgakoudi, B. C. Jacobson, J. Van Dam, V. Backman, M. B. Wallace, M. G. Muller, Q. Zhang, K. Badizadegan, D. Sun, G. A. Thomas, L. T. Perelman, and M. S. Feld, "Fluorescence, reflectance, and light-scattering spectroscopy for evaluating dysplasia in patients with Barrett's esophagus," *Gastroenterology* **120**(7), 1620–1629 (2001).
9. R. N. Graf and A. Wax, "Nuclear morphology measurements using Fourier domain low coherence interferometry," *Opt. Express* **13**(12), 4693–4698 (2005).
10. A. Wax, C. H. Yang, and J. A. Izatt, "Fourier-domain low-coherence interferometry for light-scattering spectroscopy," *Opt. Lett.* **28**(14), 1230–1232 (2003).
11. R. N. Graf, W. J. Brown, and A. Wax, "Parallel frequency-domain optical coherence tomography scatter-mode imaging of the hamster cheek pouch using a thermal light source," *Opt. Lett.* **33**(12), 1285–1287 (2008).
12. A. Wax, C. H. Yang, R. R. Dasari, and M. S. Feld, "Measurement of angular distributions by use of low-coherence interferometry for light-scattering spectroscopy," *Opt. Lett.* **26**(6), 322–324 (2001).
13. F. Robles, R. N. Graf, and A. Wax, "Dual window method for processing spectroscopic optical coherence tomography signals with simultaneously high spectral and temporal resolution," *Opt. Express* **17**(8), 6799–6812 (2009).
14. R. N. Graf and A. Wax, "Temporal coherence and time-frequency distributions in spectroscopic optical coherence tomography," *J. Opt. Soc. Am. A* **24**(8), 2186–2195 (2007).
15. A. M. Zysk, S. G. Adie, J. J. Armstrong, M. S. Leigh, A. Paduch, D. D. Sampson, F. T. Nguyen, and S. A. Boppart, "Needle-based refractive index measurement using low-coherence interferometry," *Opt. Lett.* **32**(4), 385–387 (2007).
16. A. M. Zysk, D. L. Marks, D. Y. Liu, and S. A. Boppart, "Needle-based reflection refractometry of scattering samples using coherence-gated detection," *Opt. Express* **15**(8), 4787–4794 (2007).
17. J. M. Schmitt and G. Kumar, "Turbulent nature of refractive-index variations in biological tissue," *Opt. Lett.* **21**(16), 1310–1312 (1996).
18. V. V. Tuchin, *Tissue Optics: Light Scattering Methods and Instruments for Medical Diagnosis*, SPIE Press, Bellingham, WA (2000).
19. A. Wax, C. H. Yang, V. Backman, K. Badizadegan, C. W. Boone, R. R. Dasari, and M. S. Feld, "Cellular organization and substructure measured using angle-resolved low-coherence interferometry," *Biophys. J.* **82**(4), 2256–2264 (2002).
20. F. H. White and K. Gohari, "Cellular and nuclear volumetric alterations during differentiation of normal hamster-cheek pouch epithelium," *Arch. Dermatol. Res.* **273**(3–4), 307–318 (1982).
21. Y. L. Kim, Y. Liu, R. K. Wali, H. K. Roy, and V. Backman, "Low-coherent backscattering spectroscopy for tissue characterization," *Appl. Opt.* **44**(3), 366–377 (2005).
22. H. K. Roy, Y. L. Kim, Y. Liu, R. K. Wali, M. J. Goldberg, V. Turzhitsky, J. Horwitz, and V. Backman, "Risk stratification of colon carcinogenesis through enhanced backscattering spectroscopy analysis of the uninvolved colonic mucosa," *Clin. Cancer Res.* **12**(3), 961–968 (2006).
23. Y. Liu, R. E. Brand, V. Turzhitsky, Y. L. Kim, H. K. Roy, N. Hasabou, C. Sturgis, D. Shah, C. Hall, and V. Backman, "Optical markers in duodenal mucosa predict the presence of pancreatic cancer," *Clin. Cancer Res.* **13**(15), 4392–4399 (2007).